J Radioanal Nucl Chem (2017) 313:191–196
DOI 10.1007/s10967-017-5271-5

# Time sequence determination of parent–daughter radionuclides using gamma-spectrometry

J. L. Burnett[1] · R. E. Britton[2] · D. G. Abrecht[1] · A. V. Davies[2]

Received: 8 March 2017 / Published online: 6 May 2017


**Abstract** The acquisition of time-stamped list data provides additional information useful to gamma-spectrometry analysis. A novel technique is described that uses non-linear least-squares fitting and the Levenberg–Marquardt algorithm to simultaneously determine parent-daughter atoms from time sequence measurements of only the daughter radionuclide. This has been demonstrated for the radioactive decay of short-lived radon progeny ($^{214}$Pb/$^{214}$Bi, $^{212}$Pb/$^{212}$Bi) described using the Bateman first-order differential equation. The calculated atoms are in excellent agreement with measured atoms, with a difference of 1.3–4.8% for parent atoms and 2.4–10.4% for daughter atoms. Measurements are also reported with reduced uncertainty. The technique has potential to redefine gamma-spectrometry analysis.

**Keywords** Time sequence · List mode · Gamma-spectrometry · Radon progeny

## Introduction

Advances in the digital electronics and software used in gamma-spectrometry systems are providing unprecedented possibilities for data analysis and interpretation [1–7]. A new frontier is emerging, where high-performance multichannel analyzers (MCAs) are becoming readily available at affordable cost to radiometrology laboratories. One such example is the Canberra Lynx MCA that operates pulse height analysis (PHA), multichannel scaling (MCS), multispectral scaling (MSS) and time-stamped list (TLIST) modes. The latter allows comprehensive logging of detector events with 100–200 ns timing resolution [3]. Such TLIST data is especially useful for capturing the maximum data from a measurement, and can be post-processed to provide PHA, MCS and MSS data. As the raw data is preserved, the processing can be applied on varying time-scales to identify the radioactive in-growth and decay of parent-daughter radionuclides according to their half-life (e.g. $^{214}$Pb/$^{214}$Bi, $^{212}$Pb/$^{212}$Bi, $^{140}$La/$^{140}$Ba, $^{95}$Zr/$^{95}$Nb). For a given radionuclide, these count rate changes are described by the Bateman first-order differential equations [8]. The equation can be solved using non-linear least-squares fitting and the Levenberg–Marquardt algorithm [9, 10]. The Levenberg–Marquardt algorithm was selected as it provides a more robust fitting algorithm than other methods such as the Gauss–Newton algorithm [11]. Its application herein provides a novel technique for simultaneous calculation of the parent-daughter atoms from the radioactive decay of only the daughter radionuclide.

The approach has been demonstrated using naturally occurring radionuclides (NOR) collected using a high volume air sampler. Amongst the NOR are the short-lived radon progeny ($^{214}$Pb, $^{212}$Pb, $^{214}$Bi, $^{212}$Bi, $^{218}$Po, $^{216}$Po, $^{214}$Po, $^{212}$Po and $^{208}$Tl) with half-lives ranging from $3.0 \times 10^{-7}$ s to 10.64 h [12–15]. Together with $^{222}$Rn and $^{220}$Rn, they represent 56.8% of average radiation dose received by man from natural sources [16, 17]. Their abundance in the environment and parent–daughter couplings ($^{214}$Pb/$^{214}$Bi, $^{212}$Pb/$^{212}$Bi) makes them convenient for study, and a useful proxy for other parent–daughter radionuclides that are more difficult to obtain (e.g. fission products such as $^{140}$La/$^{140}$Ba, $^{95}$Zr/$^{95}$Nb). Their accurate

✉ J. L. Burnett
jonathan.burnett@pnnl.gov

[1] Pacific Northwest National Laboratory, PO Box 999, Richland, WA, USA

[2] Atomic Weapons Establishment, Aldermaston, Reading, UK

measurement (especially for $^{220}$Rn progeny) has also often been hindered by their short half-life, highly heterogeneous distribution, low environmental concentrations and overlapping $^{222}$Rn and $^{220}$Rn distributions [18–21]. Their measurement is also important within the atmospheric sciences, as it is a major source of atmospheric ions near the earth's surface. These are important for a range of processes including nucleation of water drops necessary for rain and formation of thunderstorms [18], tracers of atmospheric transport processes [22–28], initiation of atmospheric electrical phenomena [29–31] and diffusion of solid matter [32].

## Methodology

### Experimental setup

Measurements were performed using a Canberra Broad Energy Germanium (BEGe) gamma-spectrometer (model BE6530) at the Atomic Weapons Establishment (Reading, UK). The detector was controlled by a Canberra Lynx MCA with high voltage set at +4500 V, a rise time of 5.6 us and flat top of 0.8 us. The instrument was situated within a low-background shield of aged lead (<25 Bq/kg $^{210}$Pb). Ambient radon concentrations were minimized using high laboratory air flow with HEPA filtration. Acquisition of the TLIST data was performed using the Canberra Lynx Software Development Kit and custom (C++) acquisition software written using the Microsoft Visual Studio.NET application [33]. This allows all events interacting with the BEGe to be logged to a comma-separated text file for data analysis after acquisition. The measurement sample was prepared by the collection of radon progeny (and other NOR) using a Senya Snow White air sampler with Macherey–Nagel MN85/90 filter. This was operated over a 14 day period to sample 242286.3 m$^3$ of air (with an approximate flow rate of 730 m$^3$ h$^{-1}$). After collection, the sample was promptly folded into a calibrated geometry and measured immediately for 2 days.

### Data analysis

The TLIST data was processed using custom (Visual Basic) software written using the Microsoft Visual Studio.NET application. This converted the TLIST data into a series of Canberra CAM (.cnf) format files with 4 and 30 min acquisition times. Count durations were selected for measuring the half-life of $^{214}$Pb/$^{214}$Bi and $^{212}$Pb/$^{212}$Bi respectively. The time divisions were based on the TLIST event time which is automatically corrected for dead time. The spectra were analyzed using the Canberra Genie 2000 Gamma Acquisition and Analysis software (version 3.4) to provide the net peak counts for the gamma-energies of interest (Table 1). Igor Pro (version 7.01) was then used for data analysis, including least squares fitting using the Levenberg–Marquardt algorithm. The calculated values were corrected for gamma-emission abundance, detector efficiency and true coincidence summing (TCS). The detector efficiency and TCS corrections were calculated using the Randomised Iterative Monte-Carlo Model for ENSDF Records (RIMMER) described elsewhere [34–36].

## Mathematical theory

The ($N_1$) atoms of $^{214}$Pb and $^{212}$Pb were determined from the radioactive decay of each isotope from the time sequence spectra. It was assumed that the parent $^{222}$Rn and $^{220}$Rn (and $^{218}$Po and $^{216}$Po) were removed (or decayed) during air sampling and that the lead isotopes were unsupported. As radioactive decay follows the Bateman equation:

$$N_1^t = N_1^0\left[e^{-\lambda_1 t}\right], \tag{1}$$

where $N$ represents the number of atoms at time $t$, and $\lambda_1$ is the decay constant; the gradient of a plot of $N_1^t$ versus $e^{-\lambda t}$ will equal the number of initial atoms (a linear line equation of the form $y = mx$). To calculate the daughter ($N_2$) atoms of $^{214}$Bi and $^{212}$Bi, it is necessary to consider daughter growth (and decay) from the $N_1$ parent, and the decay of the initial $N_2$ atoms. Thus, the $N_2$ atoms can be expressed as:

$$N_2^t = \frac{\lambda_1}{\lambda_2 - \lambda_1} N_1^0 (e^{-\lambda_1 t} - e^{-\lambda_2 t}) + N_2^0 e^{-\lambda_2 t}. \tag{2}$$

This equation can be manipulated to give a non-linear plane equation of the form $z = mx + ny$:

$$N_2^t = N_1^0\left[\frac{\lambda_1(e^{-\lambda_1 t} - e^{-\lambda_2 t})}{\lambda_2 - \lambda_1}\right] + N_2^0[e^{-\lambda_2 t}]. \tag{3}$$

As the equation is non-linear due to $N_2$ growth and decay from the $N_1$ parent it is not suitable for solving using multiple linear regression techniques [15, 37]. Instead non-linear least-squares data fitting using the Levenberg–

**Table 1** Gamma-energies and corrections for short-lived radon progeny

| Radionuclide | $^{214}$Pb | $^{214}$Pb | $^{214}$Bi | $^{214}$Bi | $^{212}$Pb | $^{212}$Bi |
|---|---|---|---|---|---|---|
| Half-life (seconds) | 1608 | | 1194 | | 38304 | 3633 |
| Energy (keV) | 351.9 | 295.2 | 609.3 | 1120.3 | 238.6 | 727.2 |
| Abundance (%) | 35.3 | 18.3 | 45.4 | 14.9 | 43.6 | 6.7 |
| Efficiency | 0.049 | 0.056 | 0.024 | 0.015 | 0.066 | 0.022 |
| TCS | 1.000 | 1.004 | 0.916 | 0.906 | 1.000 | 0.972 |

Marquardt algorithm was applied to fit the coefficients $m$ and $n$. The algorithm is an iterative procedure that minimizes the value of *Chi* square ($\chi^2$) from initial $m$ and $n$ guess values ($\beta$):

$$f(x^t, \beta + \delta) \approx f(x^t, \beta) + J^t \delta, \quad (4)$$

where $x^t$ is the dependent value at time $t$ ($x$ or $y$ values for parent–daughter calculations). For each iteration, the parameter $\beta$ is replaced by a new estimate $\beta + \delta$. $J^t\delta$ is the Jacobian matrix:

$$J_i = \frac{\delta f(x^t, \beta)}{\delta \beta}. \quad (5)$$

Measurement uncertainty was incorporated into the *Chi* square calculation to improve fitting and provide accurate error estimates for the fit coefficients:

$$\chi^2 = \sum_i \left( \frac{N^{\text{fit}} - N^t}{N^t_{\text{err}}} \right)^2, \quad (6)$$

where $N^{\text{fit}}$ and $N^t$ are fitted and original measurements and $N^t_{\text{err}}$ is the measurement uncertainty of the measurements.

## Results and discussion

### Parent calculations

Although solvable using linear regression, non-linear least squares fitting using the Levenberg–Marquardt algorithm was applied for ($N_1$) parent calculations from the time sequence data (Fig. 1.). This was used to validate the approach and showed excellent agreement with linear $N_1^0$ calculations (Table 2). For $^{214}$Pb, there were $4.75 \times 10^8 \pm 0.6\%$ (351.9 keV) and $4.95 \times 10^8 \pm 0.7\%$ (295.2 keV) atoms calculated, and $4.75 \times 10^8 \pm 0.6\%$ (238.6 keV) atoms for $^{212}$Pb using the Levenberg–Marquardt algorithm. Both techniques calculated the same result within 3 significant figures, and all values were within 0.07% difference. Only the uncertainty was higher using linear regression for $^{214}$Pb (295.2 keV) at 0.8% compared to 0.7% using the Levenberg–Marquardt algorithm. Decay correction of the first time sequence measurement (as for conventional analysis) was also within 1.8% (351.9 keV), 2.3% (295.2 keV) and 0.6% (238.6 keV) of the Levenberg–Marquardt calculated values. Notably, the time sequence approach significantly reduced $N_1^0$ measurement uncertainty from 1.8 to 0.6%, 2.3 to 0.7% and 0.7 to 0.2% respectively.

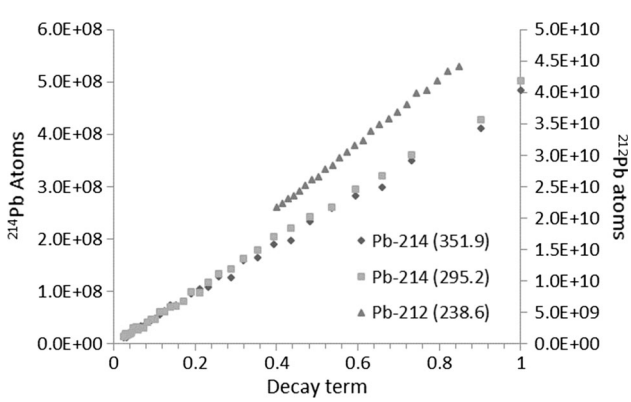


**Fig. 1** $^{214}$Pb and $^{212}$Pb time sequence measurements. The decay term is defined as $e^{-\lambda t}$. The gradient of each dataset is equal to the initial number of atoms and is solvable using the equation $y = mx$

### Parent–daughter calculations

Graphical representation of the equation $z = mx + ny$ (see Eqs. 2 and 3) shows the non-linearity associated with $N_2$ daughter growth and decay (Fig. 2). The differences in $N_1$ and $N_2$ decay terms between $^{214}$Pb/$^{214}$Bi and $^{212}$Pb/$^{212}$Bi are attributable to the half-life variations, in particular the longer-lived $^{212}$Pb ($t_{½} = 10.6$ h). Calculation of the $N_1^0$ atoms from this multidimensional $N_2$ dataset using non-linear least squares fitting (Table 3) was in good agreement with calculations from the $N_1$ dataset and measured values (compare Table 2). From the $N_2$ dataset, there were $4.60 \times 10^8 \pm 1.4\%$ $^{214}$Pb atoms and $5.18 \times 10^{10} \pm 1.1\%$ $^{212}$Pb atoms, which was within 3.2 and 0.9% of calcuations from the $N_1$ dataset, and 4.8 and 1.3% of measured values. The $N_2^0$ atoms were also calculated from the $N_2$ dataset as $6.5 \times 10^8 \pm 1.0\%$ $^{214}$Bi atoms and $5.10 \times 10^9 \pm 15.6\%$ $^{212}$Pb atoms. These values also compared well with measured values and were within 2.4 and 10.4% difference respectively. The higher uncertainty and measurement difference for $^{212}$Pb atoms is attributable to the increased $N_2$ variance. This is due to the reduced $^{212}$Bi signal caused by the lower gamma abundance (6.7% at 727.2 keV) and branching ratio (64.1%).

The $N_2^0$ calculation using the Levenberg–Marquardt algorithm can be refined by utilizing the $N_1^0$ atoms calculated from the $N_1$ decay (i.e. from the equation $y = mx$). This solves the $mx$ term of the non-linear equation $z = mx + ny$, such that least squares fitting is only required for $n$ calculation. Using this approach, and the values from Table 1, there are $6.42 \times 10^8 \pm 0.8\%$ $^{214}$Bi atoms and $4.98 \times 10^9 \pm 13.4\%$ $^{212}$Bi atoms which is within 1.0 and 9.3% of the measured values. As with the previous calculation, the increased $^{212}$Bi difference is due to the relatively high variance in the $N_2$ measurements. However, as the half-life of $^{208}$Tl is relatively short ($t_{½} = 3.05$ min) compared to the $^{212}$Bi parent, equilibrium should exist between the two isotopes during counting. Thus conversion of the $^{212}$Bi $N_2^0$ atoms to $^{208}$Tl $N_3^0$ atoms yields $2.51 \times 10^8 \pm 13.4\%$ atoms, which is within 4.0% of the measured $^{208}$Tl atoms (583.2 keV).

**Table 2** Calculated $^{214}$Pb and $^{212}$Pb atoms from the $N_1$ dataset using non-linear least squares fitting and linear regression

| Nuclide | Energy (keV) | Levenberg–Marquardt algorithm | | | Linear regression | | | Measured | |
|---|---|---|---|---|---|---|---|---|---|
| | | $N_1^0$ | ± (%) | $\chi^2$ | $N_1^0$ | ± (%) | $\chi^2$ | $N_1^0$ | ± (%) |
| $^{214}$Pb | 351.9 | 4.75E+08 | 0.6 | 39.9 | 4.75E+08 | 0.6 | 39.9 | 4.83E+08 | 1.8 |
| $^{214}$Pb | 295.2 | 4.95E+08 | 0.7 | 29.0 | 4.94E+08 | 0.8 | 29.0 | 5.01E+08 | 2.3 |
| $^{212}$Pb | 238.6 | 5.31E+10 | 0.2 | 36.3 | 5.31E+10 | 0.2 | 36.1 | 5.19E+10 | 0.6 |

Measured values are also shown for comparison

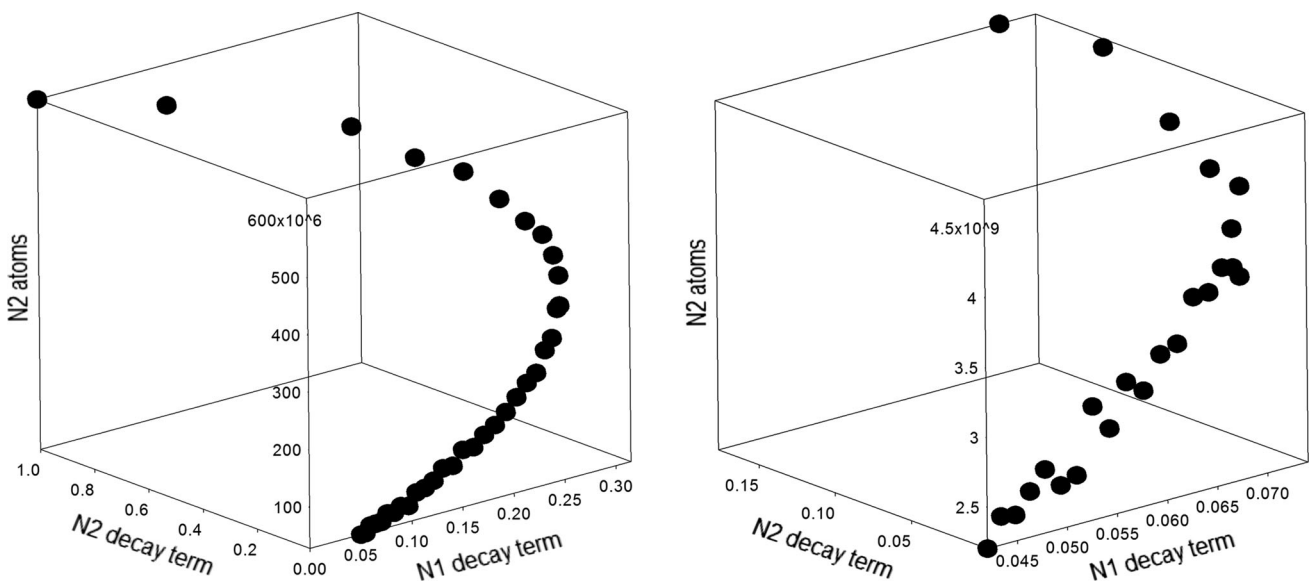


**Fig. 2** $^{214}$Bi (*left*) and $^{212}$Bi (*right*) time sequence measurements. The $N_1$ decay term is defined as $\frac{\lambda_1(e^{-\lambda_1 t}-e^{-\lambda_2 t})}{\lambda_2-\lambda_1}$ and the $N_2$ decay term as $e^{-\lambda t}$. The gradients of the curve are equal to the initial $N_1$ and $N_2$ atoms and are solvable using the equation $z = mx + ny$

**Table 3** Calculated $^{214}$Pb/$^{214}$Bi and $^{212}$Pb/$^{212}$Bi atoms from the $N_2$ dataset using non-linear least squares fitting

| Nuclide | Levenberg–Marquardt Algorithm | | | | | Measured | | | |
|---|---|---|---|---|---|---|---|---|---|
| | $N_1^0$ | ± (%) | $N_2^0$ | ± (%) | $\chi^2$ | $N_1^0$ | ± (%) | $N_2^0$ | ± (%) |
| $^{214}$Pb–$^{214}$Bi | 4.60E+08 | 1.4 | 6.51E+08 | 1.0 | 46.6 | 4.83E+08 | 1.8 | 6.35E+08 | 1.8 |
| $^{212}$Pb–$^{212}$Bi | 5.18E+10 | 1.1 | 5.10E+09 | 15.3 | 25.4 | 5.19E+10 | 0.6 | 5.45E+09 | 3.1 |

Measured values are also shown for comparison

## Other radionuclides

Future research shall apply non-linear least squares fitting and the Levenberg–Marquardt algorithm to datasets containing other parent-daughter radionuclides, including longer-lived fission products such as $^{140}$La/$^{140}$Ba and $^{95}$Zr/$^{95}$Nb. As with this NOR experiment, the TLIST data shall be split into a series of time sequence components. A potential challenge will be to obtain sufficient counts for statistically significant radionuclide identification at relatively short timescales and lower activity samples. However, this problem will be largely mitigated by optimization of the time sequence count duration for the half-life of the radionuclides of interest. Measurement of longer-lived radionuclides will also enable a larger $N_1$ and $N_2$ dataset, and this may improve the $N_1^0$ and $N_2^0$ calculation.

## Conclusions

A novel solution has been described that uses non-linear least-squares fitting and the Levenberg–Marquardt algorithm to determine parent-daughter atoms from the Bateman first-order differential equations. This has been

demonstrated using TLIST data of short-lived radon progeny ($^{214}$Pb, $^{214}$Bi, $^{212}$Pb, $^{212}$Bi) on an air filter sample. Using only $^{214}$Pb and $^{212}$Pb $N_1$ time sequence data, the initial $N_1^0$ atoms have been calculated within 0.6–2.3% of measured values with reduced measurement uncertainty. Simultaneous parent-daughter ($^{214}$Pb/$^{214}$Bi, $^{212}$Pb/$^{212}$Bi) calculation from only the $N_2$ daughter $^{214}$Bi and $^{212}$Bi time sequence data, is within 1.3–4.8% of measured values for the $N_1$ parent, and 2.4–10.4% of measured values for the $N_2$ daughter. The best agreement was for $^{214}$Pb/$^{214}$Bi calculations and also provided improvements in measurement uncertainty. This time sequence technique provides a powerful tool for radionuclide identification and quantification, with potential to redefine gamma-spectrometry analysis.

**Acknowledgements** The authors thank individuals at PNNL who have provided support at various times. This includes Michael Mayer, Michael Cantaloub, Lori Metz and Judah Friese. The views expressed here do not necessarily reflect the opinion of the United States Government, the United States Department of Energy, or the Pacific Northwest National Laboratory. Pacific Northwest National Laboratory is operated for the U.S. Department of Energy by Battelle under Contract DE-AC05-76RL01830.

## References

1. Burnett JL, Davies AV (2014) Cosmic veto gamma-spectrometry for Comprehensive Nuclear-Test-Ban Treaty samples. Nucl Instrum Methods Phys Res Sect A 747:37–40. doi:10.1016/j.nima.2014.02.027
2. Burnett JL, Davies AV (2013) Compton suppressed gamma-spectrometry for Comprehensive Nuclear-Test-Ban Treaty samples. J Radioanal Nucl Chem 295(1):497–499. doi:10.1007/s10967-012-1795-x
3. Burnett JL, Davies AV (2011) Investigating the time resolution of a compact multidimensional gamma-spectrometer. J Radioanal Nucl Chem 288(3):699–703. doi:10.1007/s10967-011-1017-y
4. Burnett JL, Davies AV, McLarty JL (2013) Further development of a cosmic veto gamma-spectrometer. J Radioanal Nucl Chem 298(2):987–992. doi:10.1007/s10967-013-2460-8
5. Burnett JL, Cantaloub MG, Mayer MF, Miley HS (2017) Development of a multidimensional gamma-spectrometer. J Radioanal Nucl Chem. doi:10.1007/s10967-017-5202-5
6. Cagniant A, Douysset G, Fontaine JP, Gross P, Petit GL (2015) An introduction to γ3 a new versatile ultralow background gamma spectrometer. Background description and analysis. Appl Radiat Isot 98:125–133. doi:10.1016/j.apradiso.2015.01.027
7. Cagniant A, Delaune O, Réglat M, Douysset G, Gross P, Le Petit G (2017) Ground surface ultralow background spectrometer: active shielding improvements and coincidence measurements for the Gamma3 spectrometer. Appl Radiat Isot. doi:10.1016/j.apradiso.2017.01.044
8. Bateman H (1910) Solution of a system of differential equations occurring in the theory of radiactive transformations. Proc Cambridge Philos Soc 15:423–427
9. Marquardt DW (1963) An algorithm for least-squares estimation of nonlinear parameters. J Soc Ind Appl Math 11(2):431–441
10. Chen L (2016) A high-order modified Levenberg–Marquardt method for systems of nonlinear equations with fourth-order convergence. Appl Math Comput 285:79–93. doi:10.1016/j.amc.2016.03.031
11. Bao J-F, Li C, Shen W-P, Yao J-C, Guu S-M (2017) Approximate Gauss–Newton methods for solving underdetermined nonlinear least squares problems. Appl Numer Math 111:92–110. doi:10.1016/j.apnum.2016.08.007
12. Burnett JL (2007) Understanding the contribution of naturally occurring radionuclides to the measured radioactivity in AWE environmental samples. University of Southampton, Southampton
13. Burnett JL, Croudace IW, Ewarwick P (2010) Short-lived variations in the background gamma-radiation dose. J Radiol Prot 30(3):525–533. doi:10.1088/0952-4746/30/3/007
14. Burnett JL, Croudace IW, Warwick PE (2012) Pre-concentration of short-lived radionuclides using manganese dioxide precipitation from surface waters. J Radioanal Nucl Chem 292(1):25–28. doi:10.1007/s10967-011-1392-4
15. Burnett JL, Croudace IW, Warwick PE (2011) Variations in the gross alpha and beta activity in surface waters at the Atomic Weapons Establishment Aldermaston (UK). J Radioanal Nucl Chem 289(2):389–394. doi:10.1007/s10967-011-1094-y
16. UNSCEAR (1988) Sources, effects and risks of ionizing radiation. United Nations Scientific Committee on the Effects of Atomic Radiation, New York
17. UNSCEAR (2000) Exposures from natural radiation sources. United Nations Scientific Committee on the Effects of Atomic Radiation, New York
18. Schery SD (1992) Thoron and its progeny in the atmospheric environment. In: Nriagu JO (ed) Gaseous pollutants: characterization and cycling. Wiley, New York, pp 423–457
19. Buzinny M, Los L (1997) Comparative measurements of radon, thoron and their daughters. Paper presented at the European Conference on Protection Against Radon at Home and at Work, Czech Republic
20. Mohamed A, El-Hussein A (2005) Comparison of outdoor activity size distributions of $^{220}$Rn and $^{222}$Rn progeny. Appl Radiat Isot 62(6):955–959
21. Winkler R, Aehlig K (1998) Temporal variation of thoron decay product concentration in the atmosphere and comparison with radon decay product concentration. Radiat Environ Biophys 37:35–39
22. Israel H (1971) Atmospheric electricity, vol 1. National Technical Information Service, Springfield
23. Israel H (1972) Atmospheric electricity, vol 2. National Technical Information Service, Springfield
24. Israel H, Horbert M, de La Riva C (1968) Measurement of the thoron concentration of the lower atmosphere in relation to the exchange ("Austausch") in this region (trans: APO USA). USA
25. Burchfield LA, Akridge JD, Kuroda PK (1983) Temporal distributions of radiostrontium isotopes and radon daughters in rainwater during a thunderstorm. J Geophys Res 88:8579–8584
26. Bigu J (1985) Theoretical models for determining $^{222}$Rn and $^{220}$Rn progeny levels in Canadian underground U mines—a comparison with experimental data. Health Phys 48:371–399
27. Willet J (1985) Atmospheric-electrical implications of $^{222}$Rn daughter deposition on vegetated ground. J Geophys Res 90:5901–5908
28. Whittlestone S, Schery SD, Li Y (1996) Pb-212 as a tracer for local influence on air samples at Mauna Loa Observatory, Hawaii. J Geophys Res 101:14777–14785
29. Israel H (1973) Atmospheric electricity. National Technical Information Service, Springfield
30. Martell EA (1985) Enhanced ion production in convective storms by transpired radon isotopes and their decay products. J Geophys Res 90:5909–5916
31. Hoppel WA, Anderson RV, Willet J (1986) Atmospheric electricity in the planetary boundary layer. The earth's electrical environment. National Academic Press, Washington, DC

32. Bigu J (1992) Metrology and monitoring of thoron ($^{220}$Rn). Mining Research Laboratories, Elliot Lake
33. Britton R, Burnett JL, Davies AV, Regan PH (2015) Coincidence corrections for a multi-detector gamma spectrometer. Nucl Instrum Methods Phys Re Sect A 769:20–25. doi:10.1016/j.nima.2014.09.054
34. Britton R, Jackson MJ, Davies AV (2015) Quantifying radionuclide signatures from a γ–γ coincidence system. J Environ Radioact 149:158–163. doi:10.1016/j.jenvrad.2015.07.025
35. Britton R, Jackson MJ, Davies AV (2016) Incorporating X–ray summing into gamma–gamma signature quantification. Appl Radiat Isot 116:128–133. doi:10.1016/j.apradiso.2016.07.019
36. Jackson MJ, Britton R, Davies AV, McLarty JL, Goodwin M (2016) An automated Monte-Carlo based method for the calculation of cascade summing factors. Nucl Instrum Methods Phys Res Sect A 834:158–163. doi:10.1016/j.nima.2016.07.016
37. Burnett JL, Croudace IW, Warwick PE (2011) Pre-concentration of naturally occurring radionuclides and the determination of $^{212}$Pb from fresh waters. J Environ Radioact 102(4):326–330. doi:10.1016/j.jenvrad.2011.01.001